COORDX: ACCELERATING IMPLICIT NEURAL REPRESENTATION WITH A SPLIT MLP ARCHITECTURE

Anonymous authors
Paper under double-blind review

ABSTRACT

Implicit neural representations with multi-layer perceptrons (MLPs) have recently gained prominence for a wide variety of tasks such as novel view synthesis and 3D object representation and rendering. However, a significant challenge with these representations is that both training and inference with an MLP over a large number of input coordinates to learn and represent an image, video, or 3D object, require large amounts of computation and incur long processing times. In this work, we aim to accelerate inference and training of coordinate-based MLPs for implicit neural representations by proposing a new split MLP architecture, *CoordX*. With CoordX, the initial layers are *split* to learn each dimension of the input coordinates separately. The intermediate features are then fused by the last layers to generate the learned signal at the corresponding coordinate point. This significantly reduces the amount of computation required and leads to large speedups in training and inference, while achieving similar accuracy as the baseline MLP. This approach thus aims at first learning functions that are a decomposition of the original signal and then fusing them to generate the learned signal. Our proposed architecture can be generally used for many implicit neural representation tasks with no additional memory overheads. We demonstrate a speedup of up to 2.92x compared to the baseline model for image, video, and 3D shape representation and rendering tasks.

1 INTRODUCTION

Recently, CoordX uses split initial layers to learn independent intermediate features of each input dimension before fusing them at the layer. These *implicit neural representations* leverage multilayer perceptrons (MLPs) to represent images, videos, 3D objects, etc (Mildenhall et al., 2020; Sitzmann et al., 2020; Tancik et al., 2020). These MLPs (coordinate-based MLPs, coordMLP for short) take low dimensional coordinates (e.g., coordinate position or time index) as input and predict the value of a learned signal (eg. color, depth, shape, etc.) of each coordinate point. The coordinate-based MLP learns an implicit, continuous, and differentiable function that maps input coordinates to various signals.

There are several benefits to using an implicit neural representation instead of a traditional discrete representation. First, it is potentially more memory efficient. Unlike the discrete representation where the granularity of the represented object is limited by the grid resolution, the granularity of a neural implicit representation can be freely adjusted by choosing different resolutions of input coordinates while not exceeding the representation capacity of the learned MLP. Second, the fully differentiable learning process allows the MLP to learn complex signals from *sparsely* available data points to reconstruct high-quality images or objects. Recent research has demonstrated the effectiveness of coordMLPs for a wide range of signal fitting or learning tasks such as image super-resolution (Chen et al., 2021), 3D shape representation (Park et al., 2019; Mescheder et al., 2019; Gropp et al., 2020), novel view synthesis (Mildenhall et al., 2020; Martin-Brualla et al., 2021; Schwarz et al., 2020) and photo-realistic 3D scene editing (Niemeyer & Geiger, 2021). The search for more accurate and generalizable implicit neural network architectures and methodologies is an active area of research.

However, a key challenge of implicit neural representation is the significant computation demand for both inference and training. For inference, the MLP has to be queried with *each* positional point

to generate the learned signal at the corresponding position. Using one GTX1080 GPU, rendering a 1024×1024 sized image on 5-layer coordMLP takes 0.2 seconds, and rendering an image of size 400×400 from a novel view with the NeRF model takes 18 seconds. Both tasks perform millions of MLP queries. Similarly, training an MLP for neural representation is a very computation intensive task as each MLP requires full training passes over a large number of sample points from the original signal. On a high end RTX GPU, it takes more than 10 minutes to learn a 512×512 image using a 5-layer coordMLP and more than 4 hours to reconstruct a low-resolution scene with NeRF.

Several recent works aim to improve the speed of inference and/or training for coordinate-based MLPs for novel view synthesis tasks (Liu et al., 2020; Neff et al., 2021; Garbin et al., 2021; Yu et al., 2021) or image/object representation (Martel et al., 2021; Takikawa et al., 2021). These works leverage spatial sparsity inherent in images, videos, and objects to reduce the amount of computation required for inference or training. For example, NSVF (Liu et al., 2020) constructs a sparse discrete representation using a voxel octree. A neural implicit representation is then learned over the discrete set of voxels instead of the infinite set of coordinates. However, there are several drawbacks to these approaches. First, they are typically applicable only to specific tasks, e.g., novel view synthesis (Neff et al., 2021). Second, the additional data structures or models that are used to explicitly save representations to avoid computation may lead to high memory overheads, e.g., Garbin et al. (2021). Third, the effectiveness of these approaches is limited by the sparsity of the signal being learned and they may be less effective for highly dense and feature-rich images/objects.

Our goal, in this work, is to accelerate both training and inference for a wide range of coordMLP-based representation tasks. To this end, we leverage the following observation. The input to these MLPs are typically multi-dimensional coordinate points, i.e., an (x, y) coordinate for an image, (x, y, t) for a video, etc., and in existing MLPs, each coordinate is processed independently, as depicted in Fig. 1(d). However, this misses the implicit locality among points in an image that have similar coordinate values, for example, the neighboring points along the same axis. In this work, we propose a new architecture where the initial layers are *split* to independently process each dimension of the input. Thus, each *dimension* is treated independently rather than each coordinate point itself. The outputs of these initial layers are then fused to generate a final prediction based on all input dimensions, as depicted in Fig. 1(e). We refer to this split architecture as *CoordX*.

The major benefits of our approach are: First, it enables significant speedups in both training and inference by essentially reducing the dimensions of the input. For example, with a image with height H and width W, the overall size of the inputs fed into the MLP is reduced from $H \times W$ to $H + W$, At the same time, by leveraging the locality between points with similar coordinate values, we are able to achieve accuracy close to the baseline architecture. Second, this technique can be applied orthogonally to previously-proposed optimization techniques that leverage sparsity and does not incur any additional memory overheads. Third, the dimension-based splitting approach can be applied to a wide range of tasks that use coordinate-based MLPs as we demonstrate in this work.

The key challenges in developing a split architecture are: (i) ensuring that the overall size of the model does not increase even when processing each dimension of the input with a separate layer; and (ii) effectively fusing features from the split layers to retain the original model accuracy. In this work, we handle these challenges by (i) splitting only the first FC layer and then sharing the remaining FC layers across all input branches; and (ii) fusing features from split branches using an outer product operation. We demonstrate that CoordX can significantly accelerate training and inference for various signal fitting tasks including image, video, and 3D shape fitting. Our analysis shows a speedup of $\sim$2.5X using a 5-layer CoordX model for various tasks. We demonstrate a 2.35x speedup in inference time for a 1k resolution image and a 2.78x speedup for a 1k resolution video clip in our experiments.

To summarize, in this work, we make the following contributions:

- We develop a new architecture for coordinate-based MLPs that leverages locality between input coordinate points to reduce the amount of computation required and significantly speed up inference and training.

- We design the split MLP architecture such that the model size is unchanged while achieving faster training and inference and retaining similar accuracy as the baseline models.

- We demonstrate CoordX's effectiveness in speeding up inference and training on various signal fitting tasks including image, video and 3D shape rendering, and other advanced applications such as image super-resolution.

2 Related Work

Coordinate-based MLPs for implicit neural representation. Recent works have demonstrated the potential of MLPs in implicitly representing signals such as images (Stanley, 2007), volume occupancy (Peng et al., 2020; Mescheder et al., 2019), signed distance (SDF) (Park et al., 2019; Xu et al., 2019), texture (Saito et al., 2019; Henzler et al., 2020), and radiance fields (NeRF) (Mildenhall et al., 2020). Unlike MLPs used for other tasks, an MLP used for implicit representation needs to be able to capture the high frequency variations in the color or geometry of images and objects. To address this, Mildenhall et al. (2020) proposes a *positional encoding* (PE) method that maps the original input coordinates into a high dimensional space using a series of high frequency functions to better capture high frequency variations. Sitzmann et al. (2020) use *sinusoidal activation* functions (SIREN) to replace the ReLU activations in the MLP, and Tancik et al. (2020) use simple Fourier feature mappings of input coordinates to learn high frequency variations. Many recent works also aim to make the signals represented by coordinate-based MLPs editable or generalizable. A common way to enrich representation power of these models is to add latent codes/features as additional inputs to the coordMLPs (Schwarz et al., 2020; Park et al., 2021; Chen et al., 2021; Mehta et al., 2021). These additional inputs are combined with positional coordinates and are essentially treated as additional dimensions in the input coordinates. CoordX is directly applicable to these works.

Accelerating MLPs for implicit neural representation. Several recent works aim to accelerate inference and/or training for implicit neural representation using MLPs. There are broadly two directions among existing works: (i) reducing the number of points to be queried; (ii) reducing the time spent in processing each point. Reducing the number of query points is a common optimization method for ray-casting based 3D neural representations. Due to spatial sparsity in a 3D scene, a significant number of sampled points along cast rays are empty, without useful density or color information. The inference/training speed can be greatly improved by skipping the processing of these points. Neff et al. (2021) use an additional depth network to estimate object depth along each ray, thus only points around the object surface are sampled. Similarly, traditional explicit 3D representation methods can be leveraged to guide point sampling. Garbin et al. (2021) and Kellnhofer et al. (2021) explicitly extract the mesh of a rendered object after training to reduce the number of points that need to be processed by the MLP. Liu et al. (2020); Yu et al. (2021); Takikawa et al. (2021) construct an octree structure to represent the 3D object during training that enables skipping empty spaces. To reduce the computation done for each point during inference, Reiser et al. (2021) replace the larger MLP for the whole scene with many tiny MLPs that have fewer layers and parameters, each of which only represents a small region of the whole scene. Garbin et al. (2021) and Yu et al. (2021) also pre-compute points and store results in memory. Therefore, only lightweight interpolation rather than intensive MLP computation is performed for each query point during rendering. To alleviate the significant memory requirements and processing time to pre-compute the original NeRF MLP's 5D input grid (3D position + 2D direction), these works leverage spherical harmonics (Ramamoorthi & Hanrahan, 2001) to generate a more efficient 3D representation.

Compared to these works, our approach is orthogonal and can be used to generate speedups in addition to those achieved by these works. Additionally, CoordX offers the following benefits. First, the splitting approach is more generally applicable to various tasks that use coordinate-based MLPs, unlike several prior works that are tailored to accelerating specific tasks, e.g., novel view synthesis. The effectiveness of CoordX is also not limited by the available sparsity in the learned object or image. Second, CoordX does not incur any additional memory overheads whereas prior works that save explicit representations may incur significant memory overheads that limit the applicability to smaller and less dense scenes, e.g., Garbin et al. (2021); Yu et al. (2021).

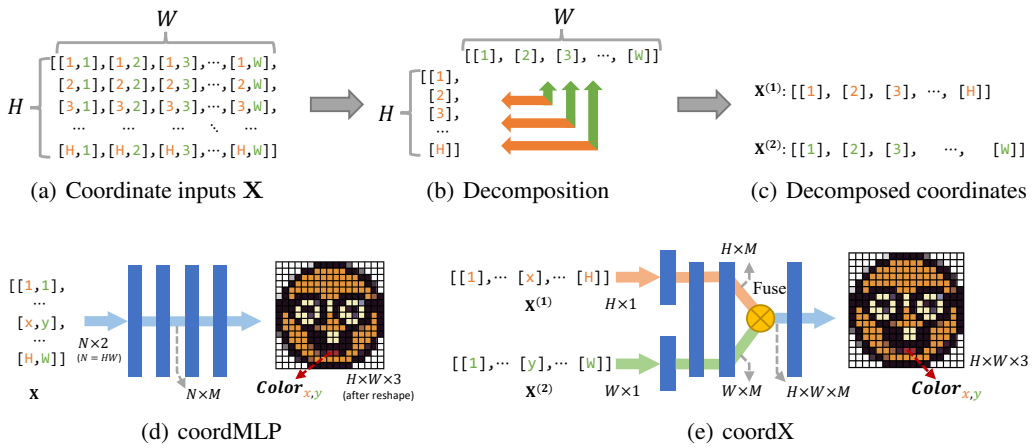

(a) Coordinate inputs $\mathbf{X}$ (b) Decomposition (c) Decomposed coordinates

(d) coordMLP (e) coordX

Figure 1: (a)-(c) The process of decomposing coordinate inputs $\mathbf{X}$ for 2D image of size $H \times W$ into 2 split parts $\mathbf{X}^{(1)}$ and $\mathbf{X}^{(2)}$. (d) Baseline coordMLP architecture. $N = HW$ coordinate inputs ($\mathbf{X}$) are independently fed into the MLP. (e) Our CoordX architecture. The initial layer is split up into separate branches for each decomposed coordinates $\mathbf{X}^{(1)}$ and $\mathbf{X}^{(2)}$. After shared FC layers, the split features are fused and the fused features are then fed into a few FC layers to generate the final signal values. M is the size of the hidden features.

3 METHOD

3.1 NEURAL NETWORK ARCHITECTURE

In our proposed architecture, the initial layer of the MLP is split across C input branches. The following $D_s - 1$ FC layers are shared among the input branches. The fusion operation then fuses the intermediate features from the different feature branches and feeds fused features to last D_f FC layers to generate the final signal values (see Fig. 1(e)).

Input decomposition along coordinate dimensions. In typical coordMLP models, a set of N coordinate points are individually queried as inputs, where $N = HW$ for an image of size $H \times W$ in Fig. 1(d). We refer to this set of input coordinate points as $\mathbf{X} \in \mathbb{R}^{N \times K}$, where K is the dimension of each point (e.g., $K = 2$ for (x, y) points on a pixel plane). With CoordX, instead of querying the first layer of the MLP with N coordinate points of dimension K, we split the first layer of the MLP into C separate branches, where $C \leq K$. If $K = C$, each dimension i of the K-D input coordinate is separately fed to the corresponding C_i input branch as shown in Fig 1(e). If $C < K$, in this case, 1 or more coordinate dimensions are not split and retained their original form. For example, coordinate points in a video (x, y, t) $(K = 3)$ can be decomposed along 2 dimensions $(C = 2)$: branch 1 is fed by 2D coordinate points along the X and Y dimensions as (x, y) and branch 2 is fed by the temporal dimension (t).

Thus the input grid $\mathbf{X} \in \mathbb{R}^{N \times K}$ is transformed into a set of decomposed input grids $\{\mathbf{X}^{(i)} \in \mathbb{R}^{B_i \times K_i} \mid i = 1, 2, \ldots, C\}$, where i is the input branch, B_i is the number of coordinate points fed into branch i and K_i is the dimension of the each decomposed coordinate point fed into branch i. Thus, $N = \prod_{i=1}^{C} B_i$ and $K = \sum_{i=1}^{C} K_i$.

First layer. The first layer of CoordX contains C parallel branches converting $\mathbf{X}^{(i)}$ to the corresponding hidden features $\mathbf{H}_1^{(i)}$. Each branch i has a weight matrix $\mathbf{W}_1^{(i)} \in \mathbb{R}^{K_i \times M}$, where M is output feature size. With activation function $\phi(\cdot)$, the first layer is [1]:

$$\{\mathbf{H}_1^{(i)} = \phi(\mathbf{X}^{(i)};\ \mathbf{W}_1^{(i)}) \mid i = 1, 2, \ldots, C\} \tag{1}$$

Layers before fusion. To avoid adding additional parameters to our model, we use the shared weight matrices (FC layers) to process hidden features from all parallel branches after the first layer (Fig. 1(e)). Suppose there are D_s layers before fusion, we can formulate these layers as:

$$\{\mathbf{H}_j^{(i)} = \phi(\mathbf{H}_{j-1}^{(i)};\ \mathbf{W}_j) \mid i = 1, 2, \ldots, C\}, \quad j = 2, \ldots, D_s \tag{2}$$

[1] We omit the bias term $\mathbf{b}$ in the following equations for readability.

This design has the following benefits: (i) no extra parameters are added because the first layer is split among the branches and the remaining layers are shared; (ii) higher computational efficiency/parallelism as features from different branches can be concatenated and processed in one batch; (iii) sharing parameters between input branches enables capturing correlations between the different input dimensions.

Feature Fusion. The intermediate features $\mathbf{H}^{(i)}_{D_s} \in \mathbb{R}^{B_i \times M}$ from the C branches are then combined to generate a fused feature $\mathbf{H}^{*}_{D_s} \in \mathbb{R}^{B_1 \times \cdots \times B_C \times M}$.

We use an outer product as the fusion operation (discussed in more detail in 3.3). The fusion operation is formulated as follows:

$$\mathbf{H}^{*}_{D_s, p_1 p_2 \ldots p_C} = \text{Fuse}(\mathbf{H}^{(1)}_{D_s}, \cdots, \mathbf{H}^{(C)}_{D_s}) = \prod_{i=1}^{C} \mathbf{H}^{(i)}_{D_s, p_i} \tag{3}$$

p_i is the positional index for feature tensors. We use $\prod_{\mathbf{i=1}}^{\mathbf{C}} \mathbf{X_i}$ to denote a series of outer products over the terms $\mathbf{X_i}$ The last D_f FC layers from the baseline model are retained to transform the fused features into final predictions.

Speedup Analysis. We assume each FC layer of the coordinate-based MLP has the same amount of computation. In a D-layer baseline coordMLP, there are N coordinate inputs processed by each layer of the MLP. The resulting computation is of the order $\mathcal{O}(DN)$. In a D-layer CoordX model with C split branches, we assume B_i (the number points processed by branch i) equals B, thus $N = \prod_{i=1}^{C} B_i = B^C$. Each of the C branches from the first D_s layers before fusion needs to process B decomposed inputs and the remaining D_f layers ($D_s + D_f = D$) process the fused features of the original size N. The two parts in CoordX together result in computation of the order $\mathcal{O}(CD_sB + D_fN)$. The ratio γ of the computational complexity between the two methods is

$$\gamma = \frac{DN}{CD_sB + D_fN} = \frac{(D_s + D_f)B^C}{CD_sB + D_fB^C} = \frac{\lambda + 1}{\lambda CB^{1-C} + 1}, \quad \lambda = \frac{D_s}{D_f} \tag{4}$$

When B is large enough, the term λCB^{1-C} becomes negligibly small. Thus, the theoretical upper bound of the speedup that can be achieved is $\gamma \rightarrow \lambda + 1$. A 5-layer CoordX MLP with $D_s = 3$ and $D_f = 2$ can thus achieve a 2.5x speedup over a 5-layer baseline MLP based on our assumptions.

3.2 Accelerating Training with CoordX

When the input coordinates are split along each coordinate dimension, during the fusion stage, the original coordinates are reconstructed by simply generating all combinations of the input values along each dimension. Thus, to perform this splitting for training, the original signal values must be available for all combinations of the split inputs. However, typically in a training pipeline, input points are randomly chosen and all combinations will not be available. To address this, we select a subset of points such that these points can be split along each dimension, and the overall subset can be reconstructed with combinations of the split inputs. We discuss how this is done in more detail in Appendix A. It should be noted that training with randomly sampled points can also be done with the split architecture. However, in this case, the input points need to be processed individually, leading to slowdowns compared to the baseline MLP.

3.3 The signal decomposition of CoordX.

Signals such as images can be decomposed into multiple matrices using mathematical methods. For example, a gray-scale image (represented as a 2D matrix) can be decomposed into two matrices using an SVD or QR decomposition. Similarly, our proposed split architecture can essentially be thought of as learning multiple matrices that are then used to reconstruct the original signal, as depicted in Fig. 2. By moving the fusion operation (outer product) to the end of the model ($D_f = 0$), we get a fully split CoordX model. This fully split CoordX model is also able to represent the image with high PSNR (Fig. 2(b)), indicating the ability of the model to learn decomposed signals.

A key difference between the previously-presented CoordX model (e.g., Fig. 1(e)) and the fully split CoordX model (e.g., Fig. 2(a)) is the location of the fusion operation. Our fusion operation

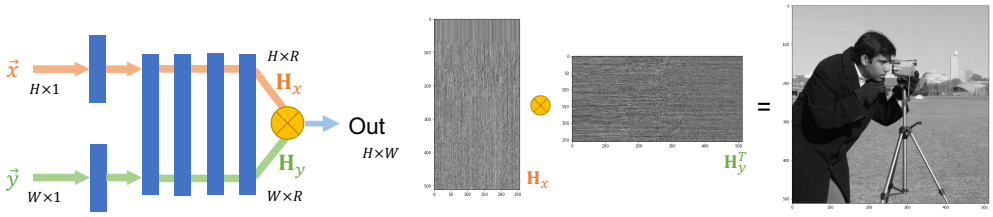

(a) Fully split CoordX (b) Decomposed image matrices

Figure 2: CoordX learns the image decomposition. (a) The fully split coordX architecture. The fusion operator directly generates the predicted signal. R is the dimension reduced by the summation after the outer product. (b) The image can be represented as a matrix multiplication between two learned feature tensors (matrices) $\mathbf{H}_x$ and $\mathbf{H}_y$. $R = 256$, $H = W = 512$ in this example.

defined in Eqn. 3 is a series of outer product, while the fully split CoordX in Fig. 2 requires an outer product to generate the final prediction without an additional FC layer. In order to include these two cases in one fusion equation, we extend the dimension of the split features to be fused. Let the hidden features after D_s layers be of feature size M. The M hidden feature values then can be reshaped into a $R \times S$ matrix (where $M = RS$). R is the size of the dimension reduced by the summation after outer product, and S represents the feature/signal size after the fusion. For example, $R = 1, S = M$ for fusion in the partially-split CoordX. The fully split CoordX in Fig. 2 has $R = 256$ and $S = 1$ (single channel image). Following our definition in 3.1, each branch's hidden feature $\mathbf{H}^{(i)} \in \mathbb{R}^{B_i \times M}$ before the fusion can be reshaped into $\mathbf{H}'^{(i)} \in \mathbb{R}^{B_i \times R \times S}$. The fusion then can be formulated as

$$\mathbf{H}^*_{p_1 p_2 \cdots p_C} = \sum_{i=1}^{R} \prod_{j=1}^{C} \mathbf{H}'^{(j)}_{p_j, i} \tag{5}$$

p_i is positional index for feature tensors, i is the index for dimension R of $\mathbf{H}'^{(i)}$, $\mathbf{H} \in \mathbb{R}^{B_1 \times \cdots \times B_C \times S}$. The fusion operation defined in Eqn. 3 is a special case of Eqn. 5 when $R = 1$. While $R = 1$ is sufficient to learn an accurate representation for most signals, if we set $R > 1$ (e.g., R is 2 or 3) for the hidden feature fusion and enlarge the corresponding FC layers by a scale factor R to keep S unchanged, the representation accuracy of the CoordX model can be improved (evaluated in Sec. 4.4).

4 Experimental Evaluation

In this section, we evaluate the performance and efficiency of CoordX for several signal fitting tasks including images, videos and 3D shapes. We also evaluate CoordX for latent code coordMLPs.

Setup. We choose several existing coordMLP models as baseline models for different tasks (details are in following subsections). All models are implemented on PyTorch (Paszke et al., 2019) and evaluated using an NVIDIA RTX3090 GPU. We use SIREN to denote models with periodic activation functions (Sitzmann et al., 2020), and we use PE to denote models using positional encoding with ReLU activation (Mildenhall et al., 2020; Tancik et al., 2020). Unless otherwise specified, our experiments use 5-layer MLPs. The CoordX models have two FC layers after the fusion operation ($D_f = 2$). Model hyperparameters such as learning rate, batch size, number of epochs, etc. are the same as those used in the corresponding baseline coordMLPs. The output image/object visualizations and qualitative comparisons are in Appendix B.

4.1 Signal Fitting with CoordX

Image Representation. In this experiment, 5-layer coordMLPs with 256 hidden units are used to fit RGB images of size 512×512. We randomly select 12 center-cropped images from DIV2K dataset (Agustsson & Timofte, 2017) to report average PSNR. Both SIREN and PE models are tested. Table 1 shows the PSNR and the required training time for 20,000 epochs. Fig. 3(a) compares the inference speed between the baseline SIREN model and CoordX for different image sizes.

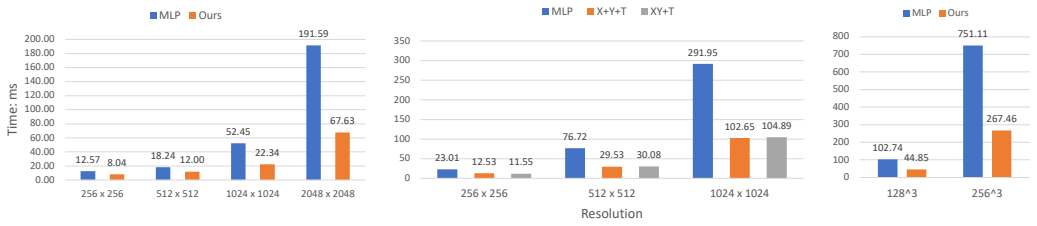

(a) Image inference (b) Video inference (c) Shape inference

Figure 3: Comparing inference speed. (a) average inference time for the SIREN model for a synthetic image on different resolutions; (b) millisecond per frame to represent a synthetic video with 100 frames on different resolutions with PE models; (c) inference time of a grid of coordinate points for marching cubes to display 3D shapes; SIREN models are used.

Method	MLP-S	CoordX-S	CoordX-S-A	MLP-P	CoordX-P	CoordX-P-A
PSNR	40.25	37.08	37.02	37.30	33.89	33.84
T_{training} (min)	12.07	22.33	5.73	14.80	27.08	5.06

Table 1: Accuracy and speed comparison. MLP indicates the baseline coordMLP. S and P refer to SIREN and PE respectively. A refers to accelerated training with our sampling method (Sec. 3.2).

We make the following observations. First, CoordX can achieve high PSNR values similar to those achieved by the corresponding baseline coordMLPs, with a slight drop in quality (we discuss ways to alleviate this in 4.4). Second, training the CoordX model is almost twice as fast as training the baseline coordMLP. Third, CoordX achieves significantly faster inference times compared to the baseline (up to 2.83x for a 2048×2048 image). The observed speedups are higher for bigger images.

Video Representation. In this task, we use 5-layer coordMLPs with 1024 hidden units to learn 10-second video clips. We evaluate 2 video clips. The baseline MLPs are described in Appendix B.

For the CoordX model, we consider two splitting strategies. The first one is to split the input coordinates into 3 vectors along the height, width, and time axes, resulting in 3 network branches (referred to as X+Y+T). The second strategy splits the input coordinates along the spatial and temporal dimensions (2 branches). The height and width dimensions are flattened into one input branch and the time dimension is the second branch. We refer to this stategy as XY+T. We use the PE method in this experiment as it performs better than SIREN for videos. Table 2 shows the average PSNR and the required training time for 100,000 epochs. Fig. 3(b) compares the inference speed between the baseline model and CoordX for different frame resolutions.

We make the following observations. First, while both X+Y+T and XY+T splitting strategies achieve high PSNR, XY+T performs slightly better than X+Y+T and even outperforms the baseline model. Second, training CoordX with our sampling strategy (XY+T-A) is 2.02X faster than training the baseline model, while retaining high representation quality in the model. Third, CoordX achieves a 2.78x speedup over the baseline MLP for inference and the speedups are higher for higher video resolutions.

3D shape representation. We choose occupancy networks (Mescheder et al., 2019) to represent 3D shapes. The output probabilities indicate whether query points are inside or outside the shape. We use 5-layer coordMLPs with 256 hidden units for this experiment and the SIREN method as it performs better than PE.

We use IoU as the quality metric (see details in Appendix B) and report the average IoU obtained for 4 3D objects. Table 2 shows the average IoU values and the required training time for 10,000 epochs. To display shapes and compare inference speeds after training, we use the marching cube[2] (Lorensen & Cline, 1987) process in which a 3D voxel grid needs to be queried. Fig. 3(c) compares the inference speed for different grid resolutions.

We make the following observations. First, we achieve similar IoU scores with CoordX compared to the baseline coordMLPs. Second, CoordX is up to 1.7x faster for training speedup compared to the

[2]Volumetric rendering, as another way to display 3D shapes, will be discussed in Appendix C.

baseline model. Third, CoordX achieve a speedup of up to 2.81x over the baseline for a resolution of 256^3 and on average 2.55x.

Task	Video				3D shape		
Method	MLP	X+Y+T	XY+T	XY+T-A	MLP	CoordX	CoordX-A
Metric	33.315	31.69	33.63	33.35	0.991 / 0.970	0.991 / 0.970	0.989 / 0.964
T_{training}	4.30 h	6.63 h	5.22 h	2.13 h	5.72 min	16.14 min	3.28 min

Table 2: Accuracy and speed comparison for MLP training. MLP indicates the baseline coordMLP. A refers to training CoordX with our sampling strategy. Video task uses PSNR as the metric, and 3D shape task uses easy / hard IoU (higher is better) as metrics.

In summary, we demonstrate that the CoordX models are able to provide significant speedups in both training and inference over baseline models for different sets of tasks. We also demonstrate that the CoordX models are able to retain the representation quality of the baseline models.

4.2 CoordX with Latent Codes

In this part, we test our method on more complex coordinate-based MLPs, which include high-dimensional latent codes as a part of the model input for better generalizability. The model we accelerate is LIIF (Local Implicit Image Function) (Chen et al., 2021) for image super-resolution. It takes a 2D pixel position and a high-dimensional LIIF latent code from a CNN encoder as inputs and then predicts the RGB value at the corresponding pixel coordinate. The coordMLP (decoder) here is a 5-layer MLP with 256 hidden units. We use a CoordX model with 4 branches (code,x,y,cell) to replace the baseline coordMLP for this task, where cell is an additional 2D input introduced in Chen et al. (2021) for better accuracy. We use a pretrained EDSR (Lim et al., 2017) decoder and train our CoordX decoder from scratch for 1,000 epochs. We use the DIV2K dataset (Agustsson & Timofte, 2017) for quantitative comparisons. Table 3 compares the baseline LIIF and our modified CoordX LIIF on different up-sampling scales, including scales used in training and not used in training.

We observe that the CoordX LIIF model achieves almost the same PSNR in compared to the original baseline model. At the same time, CoordX achieves significant speedups (up to 2.88x) for inference for a target 2K image super resolution. Since the MLP only forms a part of the overall training pipeline, CoordX does not generate significant speedups for training. We conclude that CoordX is more generally applicable to variations and enhancements of coordinate-based MLPs.

Method	In-distribution			Out-of-distribution					Speed
Up-sampling scales	$\times 2$	$\times 3$	$\times 4$	$\times 6$	$\times 12$	$\times 18$	$\times 24$	$\times 30$	($\times 2$)
EDSR-baseline-LIIF	34.67	30.96	29.00	26.75	23.71	22.17	21.18	20.48	131.03 ms
EDSR-CoordX-LIIF	34.65	30.95	28.99	26.67	23.60	22.08	21.10	20.42	45.53 ms

Table 3: Accuracy and speed comparison for MLP inference. PSNR is used as the quantitative metric. (Scores for EDSR-baseline-LIIF are from the original paper.) The speed here is the average time to finish processing all images in the DIV2K valid set with $\times 2$ scale.

4.3 The Degree of Splitting for MLP

CoordX models can be partly split or fully split (Sec. 3.3) and in this section, we evaluate the impact of different degrees of splitting for 3D shape fitting. We treat the number of layers after fusion as a hyperparameter (D_f) to be swept. We vary D_f from 0 to 5 for the 5-layer CoordX models evaluated. Note that when $D_f = 5$ the coordX model is essentially a baseline coordMLP. To demonstrate that similar representation accuracies as CoordX cannot be obtained by simply using MLPs with fewer layers, we also evaluate baseline coordMLPs with different model depth (D_{MLP}). All CoordX models use our sampling strategy (Sec. 3.2) during training. We use a 128^3 grid of coordinate points to test the inference speed. The test results are listed in Table 4.

We make the following observations. First, as we have more split layers (D_f is lower), the IoU score decreases slightly. This indicates a tradeoff between representation accuracy and training/inference speed. Second, from the our comparison with smaller baseline MLP models, we observe that similar representation accuracies cannot be obtained by simply using fewer layers (which may be faster).

Model setting	D_f						D_{MLP}		
	5*	4	3	2	1	0	4	3	2
IoU	0.976	0.980	0.974	0.963	0.941	0.880	0.959	0.876	0.516
T_{training} (min)	5.72	5.40	4.24	3.28	2.27	2.38	4.44	3.11	1.67
$T_{\text{inference}}$ (ms)	105.22	95.43	69.37	46.25	19.73	22.18	82.12	55.21	30.77

Table 4: Accuracy and speed comparison. When $D_f = 5$, CoordX becomes the baseline coordMLP.

4.4 Improving Representation Quality

As observed in Section 4.1, CoordX leads to significant speedups but causes a small drop in accuracy (3 PNSR points) specifically for image representation. Compared to other types of signals, image signals typically have more high frequency variations. The decomposition of inputs in CoordX may lead to loss of information in capturing these high frequency signal variations.

To improve the representation quality of CoordX as discussed in Section 3.3, we increase the size R of the reduction dimension ($R = 1$ for above evaluated models) and keep the fused feature size S unchanged ($S = 256$ for image models). We increase R to 2 and 3 in this evaluation and extra parameters are thus added to the splitting FC layers. This can be done in two ways. First, we can increase the number of hidde units in the layer just before fusion by a factor of R (referred to as +). Alternatively, we can increase the feature size of each splitting layer before fusion by a factor of R (referred to as ++). This approach requires the use of more parameters.

We use SIREN models for this experiment and the experimental settings are the same as in 4.1 except that all models are trained for 20,000 epochs to ensure convergence. Table 5 compares the different model configurations.

Model	MLP	CoordX	R2+	R2++	R3+	R3++
PSNR	40.25	37.08	39.70	41.32	41.60	43.55
Training time (min)	12.60	5.87	7.67	7.87	9.00	9.33
Inference speed (ms)	52.45	22.34	29.24	34.92	30.05	37.73
Model size (MB)	0.77	0.77	1.02	2.27	1.27	4.78

Table 5: Image fitting with larger CoordX models. The inference speed is the average time to inference a synthetic 1024x1024 image 100 times.

From Table 5, we make the following observations. First, increasing R can effectively improve the representation quality. The augmented CoordX models are also able to achieve higher PSNR than the baseline coordMLPs. Second, even though more parameters are added to the augmented CoordX models, the training and inference speeds are still faster than the baseline coordMLP. Third, for the same R, the R++ strategy which requires more parameters is more effective. However, increasing the R value is more beneficial compared using more parameters with the R++ strategy.

5 Conclusion and Future Work

In this work, we propose CoordX, a new architecture accelerating inference and training of coordinate-based MLPs for implicit neural representations. CoordX decomposes input positional(-temporal) coordinates along each input dimension and split the baseline MLP into a multi-branch MLP. Decomposed inputs separately feed into each branch leading to significant speedups in inference and training while retaining similar representation accuracy as the slower baseline models. We also demonstrate approaches to increase the representation capacity of a split coordinate-based MLP, leading to new design space for trading off speed, quality and size.

CoordX also has wider applicability beyond the tasks evaluated. For example, the splitting strategy introduced in this work can also be applied to accelerate view synthesis for dynamic scenes (Peng et al., 2021; Li et al., 2021), and deformable scenes (Park et al., 2020; 2021). CoordX has limited effectiveness when the input coordinates cannot be easily decomposed along input dimensions, e.g., NeRF's ray-casting sampling. We discuss a simple solution for NeRF in Appendix C and we leave further exploration of this limitation to future work. Lastly, the split MLPs proposed in this work can potentially be used for signal decomposition to learn smaller signals that can be used to reconstruct the original signal. We leave the exploration of such use cases (e.g., data compression or multi-relational data modeling (Rabanser et al., 2017)) to future work.

REFERENCES

Eirikur Agustsson and Radu Timofte. Ntire 2017 challenge on single image super-resolution: Dataset and study. In *Proceedings of the IEEE conference on computer vision and pattern recognition workshops*, pp. 126–135, 2017.

Yinbo Chen, Sifei Liu, and Xiaolong Wang. Learning continuous image representation with local implicit image function. In *Proceedings of the IEEE/CVF Conference on Computer Vision and Pattern Recognition*, pp. 8628–8638, 2021.

Stephan J Garbin, Marek Kowalski, Matthew Johnson, Jamie Shotton, and Julien Valentin. Fastnerf: High-fidelity neural rendering at 200fps. *arXiv preprint arXiv:2103.10380*, 2021.

Amos Gropp, Lior Yariv, Niv Haim, Matan Atzmon, and Yaron Lipman. Implicit geometric regularization for learning shapes. *arXiv preprint arXiv:2002.10099*, 2020.

Philipp Henzler, Niloy J Mitra, and Tobias Ritschel. Learning a neural 3d texture space from 2d exemplars. In *Proceedings of the IEEE/CVF Conference on Computer Vision and Pattern Recognition*, pp. 8356–8364, 2020.

James T Kajiya and Brian P Von Herzen. Ray tracing volume densities. *ACM SIGGRAPH computer graphics*, 18(3):165–174, 1984.

Petr Kellnhofer, Lars C Jebe, Andrew Jones, Ryan Spicer, Kari Pulli, and Gordon Wetzstein. Neural lumigraph rendering. In *Proceedings of the IEEE/CVF Conference on Computer Vision and Pattern Recognition*, pp. 4287–4297, 2021.

Diederik P Kingma and Jimmy Ba. Adam: A method for stochastic optimization. *arXiv preprint arXiv:1412.6980*, 2014.

Tianye Li, Mira Slavcheva, Michael Zollhoefer, Simon Green, Christoph Lassner, Changil Kim, Tanner Schmidt, Steven Lovegrove, Michael Goesele, and Zhaoyang Lv. Neural 3d video synthesis. *arXiv preprint arXiv:2103.02597*, 2021.

Bee Lim, Sanghyun Son, Heewon Kim, Seungjun Nah, and Kyoung Mu Lee. Enhanced deep residual networks for single image super-resolution. In *Proceedings of the IEEE conference on computer vision and pattern recognition workshops*, pp. 136–144, 2017.

Lingjie Liu, Jiatao Gu, Kyaw Zaw Lin, Tat-Seng Chua, and Christian Theobalt. Neural sparse voxel fields. *arXiv preprint arXiv:2007.11571*, 2020.

William E Lorensen and Harvey E Cline. Marching cubes: A high resolution 3d surface construction algorithm. *ACM siggraph computer graphics*, 21(4):163–169, 1987.

Julien NP Martel, David B Lindell, Connor Z Lin, Eric R Chan, Marco Monteiro, and Gordon Wetzstein. Acorn: Adaptive coordinate networks for neural scene representation. *arXiv preprint arXiv:2105.02788*, 2021.

Ricardo Martin-Brualla, Noha Radwan, Mehdi SM Sajjadi, Jonathan T Barron, Alexey Dosovitskiy, and Daniel Duckworth. Nerf in the wild: Neural radiance fields for unconstrained photo collections. In *Proceedings of the IEEE/CVF Conference on Computer Vision and Pattern Recognition*, pp. 7210–7219, 2021.

Ishit Mehta, Michaël Gharbi, Connelly Barnes, Eli Shechtman, Ravi Ramamoorthi, and Manmohan Chandraker. Modulated periodic activations for generalizable local functional representations. *arXiv preprint arXiv:2104.03960*, 2021.

Lars Mescheder, Michael Oechsle, Michael Niemeyer, Sebastian Nowozin, and Andreas Geiger. Occupancy networks: Learning 3d reconstruction in function space. In *Proceedings of the IEEE/CVF Conference on Computer Vision and Pattern Recognition*, pp. 4460–4470, 2019.

Ben Mildenhall, Pratul P Srinivasan, Matthew Tancik, Jonathan T Barron, Ravi Ramamoorthi, and Ren Ng. Nerf: Representing scenes as neural radiance fields for view synthesis. In *European conference on computer vision*, pp. 405–421. Springer, 2020.

Thomas Neff, Pascal Stadlbauer, Mathias Parger, Andreas Kurz, Joerg H Mueller, Chakravarty R Alla Chaitanya, Anton Kaplanyan, and Markus Steinberger. Donerf: Towards real-time rendering of compact neural radiance fields using depth oracle networks. *arXiv preprint arXiv:2103.03231*, 2021.

Michael Niemeyer and Andreas Geiger. Giraffe: Representing scenes as compositional generative neural feature fields. In *Proceedings of the IEEE/CVF Conference on Computer Vision and Pattern Recognition*, pp. 11453–11464, 2021.

Jeong Joon Park, Peter Florence, Julian Straub, Richard Newcombe, and Steven Lovegrove. Deepsdf: Learning continuous signed distance functions for shape representation. In *Proceedings of the IEEE/CVF Conference on Computer Vision and Pattern Recognition*, pp. 165–174, 2019.

Keunhong Park, Utkarsh Sinha, Jonathan T Barron, Sofien Bouaziz, Dan B Goldman, Steven M Seitz, and Ricardo Martin-Brualla. Deformable neural radiance fields. *arXiv preprint arXiv:2011.12948*, 2020.

Keunhong Park, Utkarsh Sinha, Peter Hedman, Jonathan T Barron, Sofien Bouaziz, Dan B Goldman, Ricardo Martin-Brualla, and Steven M Seitz. Hypernerf: A higher-dimensional representation for topologically varying neural radiance fields. *arXiv preprint arXiv:2106.13228*, 2021.

Adam Paszke, Sam Gross, Francisco Massa, Adam Lerer, James Bradbury, Gregory Chanan, Trevor Killeen, Zeming Lin, Natalia Gimelshein, Luca Antiga, et al. Pytorch: An imperative style, high-performance deep learning library. *Advances in neural information processing systems*, 32: 8026–8037, 2019.

Sida Peng, Yuanqing Zhang, Yinghao Xu, Qianqian Wang, Qing Shuai, Hujun Bao, and Xiaowei Zhou. Neural body: Implicit neural representations with structured latent codes for novel view synthesis of dynamic humans. In *Proceedings of the IEEE/CVF Conference on Computer Vision and Pattern Recognition*, pp. 9054–9063, 2021.

Songyou Peng, Michael Niemeyer, Lars Mescheder, Marc Pollefeys, and Andreas Geiger. Convolutional occupancy networks. In *Computer Vision–ECCV 2020: 16th European Conference, Glasgow, UK, August 23–28, 2020, Proceedings, Part III 16*, pp. 523–540. Springer, 2020.

Stephan Rabanser, Oleksandr Shchur, and Stephan Günnemann. Introduction to tensor decompositions and their applications in machine learning. *arXiv preprint arXiv:1711.10781*, 2017.

Ravi Ramamoorthi and Pat Hanrahan. An efficient representation for irradiance environment maps. In *Proceedings of the 28th annual conference on Computer graphics and interactive techniques*, pp. 497–500, 2001.

Christian Reiser, Songyou Peng, Yiyi Liao, and Andreas Geiger. Kilonerf: Speeding up neural radiance fields with thousands of tiny mlps. *arXiv preprint arXiv:2103.13744*, 2021.

Shunsuke Saito, Zeng Huang, Ryota Natsume, Shigeo Morishima, Angjoo Kanazawa, and Hao Li. Pifu: Pixel-aligned implicit function for high-resolution clothed human digitization. In *Proceedings of the IEEE/CVF International Conference on Computer Vision*, pp. 2304–2314, 2019.

Katja Schwarz, Yiyi Liao, Michael Niemeyer, and Andreas Geiger. Graf: Generative radiance fields for 3d-aware image synthesis. *arXiv preprint arXiv:2007.02442*, 2020.

Vincent Sitzmann, Julien Martel, Alexander Bergman, David Lindell, and Gordon Wetzstein. Implicit neural representations with periodic activation functions. *Advances in Neural Information Processing Systems*, 33, 2020.

Kenneth O Stanley. Compositional pattern producing networks: A novel abstraction of development. *Genetic programming and evolvable machines*, 8(2):131–162, 2007.

Towaki Takikawa, Joey Litalien, Kangxue Yin, Karsten Kreis, Charles Loop, Derek Nowrouzezahrai, Alec Jacobson, Morgan McGuire, and Sanja Fidler. Neural geometric level of detail: Real-time rendering with implicit 3d shapes. In *Proceedings of the IEEE/CVF Conference on Computer Vision and Pattern Recognition*, pp. 11358–11367, 2021.

Matthew Tancik, Pratul P Srinivasan, Ben Mildenhall, Sara Fridovich-Keil, Nithin Raghavan, Utkarsh Singhal, Ravi Ramamoorthi, Jonathan T Barron, and Ren Ng. Fourier features let networks learn high frequency functions in low dimensional domains. *arXiv preprint arXiv:2006.10739*, 2020.

Qiangeng Xu, Weiyue Wang, Duygu Ceylan, Radomir Mech, and Ulrich Neumann. Disn: Deep implicit surface network for high-quality single-view 3d reconstruction. *arXiv preprint arXiv:1905.10711*, 2019.

Alex Yu, Ruilong Li, Matthew Tancik, Hao Li, Ren Ng, and Angjoo Kanazawa. Plenoctrees for real-time rendering of neural radiance fields. *arXiv preprint arXiv:2103.14024*, 2021.

A INPUT POINT SAMPLING FOR COORDX TRAINING

Randomly sampling points for MLP training will not lead to any speedups with CoordX. This is because randomly chosen coordinates cannot be decomposed into input vectors along each dimension. For example, in an image if the points $[(1,1),(2,2),(3,3),(4,4)]$ are sampled, they cannot be split into two input vectors along each coordinate dimension. This is because some combinations of the input vectors are missing, e.g., $(1,3),(1,4),\ldots$ However, if points $[(1,1),(1,2),(2,1),(2,2)]$ are sampled, we can then split them into two $[(1),(2)]$ vectors along each dimension.

Thus, we need a new sampling strategy that ensures that the chosen points can be split along each coordinate dimension. To ensure this, we need to select all input points that are a combinations of the split input vectors. To this end, we formulate a simple sampling strategy that we describe below.

Suppose we need to sample N points to learn the signal bounded in a C-D coordinate space, where each dimension i is of length S_i. We assume that the number of sampled positions along each coordinate dimension is approximately proportional to the dimension length S_i, so we can represent the number of sampled positions along each dimension as μS_i, where μ is a scale factor. Because we require original sampling and our new sampling should have approximately the same number of sampled points in the same setting, we have:

$$\prod_{i=1}^{C} \mu S_i \approx N \tag{6}$$

By solving this equation, we can get

$$\mu = \sqrt[C]{\frac{N}{V}}, \quad V = \prod_{i=1}^{C} S_i \tag{7}$$

Though we limit the flexibility of sampling process, the probability of choosing a particular point/region is the same for two sampling methods. To introduce more randomness to our sampling method, we also add a random noise to each μS_i. Note that the sampled coordinate space can be continuous or discrete, but this split sampling method works in the same way.

As a result, this strategy ensures that the points selected can be fully decomposed along any dimensions. All input points that are formed when the coordinates are fused are thus selected for training. This is depicted in Fig. 4.

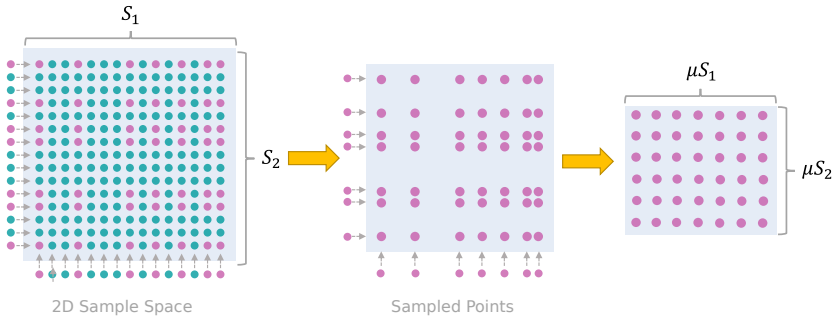

Figure 4: An illustration of our point sampling strategy in 2-D space. The data scale is S_1, S_2 on the first and second dimension, our new sampling strategy ensures that the proportions of samples along each coordinate dimension are exactly the same and can be split along each dimension.

B ADDITIONAL TASK DETAILS

In this section, we provide additional details and results regarding various fitting tasks evaluated in Section 4. All experiments on signal fitting tasks are implemented using PyTorch and use an NVIDIA RTX3090 GPU. We use the Adam optimizer (Kingma & Ba, 2014) during training.

B.1 IMAGE FITTING

This task involves training the model to fit 2D images. Given a 2D pixel coordinate, the model predicts the color of the pixel at that coordinate. One of the biggest advantages of using implicit representations is that it can represent images with an arbitrary resolution, since it learns a continuous representation of the image, therefore it can represent an image at high resolution but with a size smaller than the image itself. We formulate this task as:

$$\Phi : \mathbb{R}^2 \mapsto \mathbb{R}^O \tag{8}$$

Where O is the dimension of the pixel color value of the image, for example $O = 3$ if image is represented in RGB value, or $O = 1$ if it is a greyscale image.

In this experiment, we try to fit RGB images of size 512×512. We randomly select 12 center-cropped images from DIV2K dataset (Agustsson & Timofte, 2017) for this experiment, and train for 20,000 epochs.

In the image fitting tasks using PE, positional encoding maps input point $\mathbf{x} \in \mathbb{R}^K$ that is normalized to the range $[-1, 1]$ to $\mathbb{R}^{2Kd+K}$ using a set of sinusoidal functions:

$$\gamma(p) = (\sin(2^0\pi p), \cos(2^0\pi p), ..., \sin(2^{d-1}\pi p), \cos(2^{d-1}\pi p)) \tag{9}$$

Where K is the dimension of each input point, p is an individual coordinate in input point $\mathbf{x}$, and d is the encoding frequency. We then concatenate this encoding with the original input $\mathbf{x} \in \mathbb{R}^K$, to get an input of dimension $2Kd + K$. We follow the settings and the encoding frequency used in the image fitting task introduced in (Tancik et al., 2020).

We separately sample 2D pixel coordinates on each axis. We sample 512 points from both axis for each training batch. Since the image size are 512×512, we can fit all sampled points into one batch on a RTX3090 GPU.

In Fig 5, we choose 4 images of various complexities from the DIV2K dataset to show the qualitative results for the image fitting task.

B.2 VIDEO FITTING

We also train our model to learn video representations. Compared to images, videos have an extra dimension which is the temporal dimension or the frame number. Therefore this fitting task has an input of 3D coordinates (x, y, t) where (x, y) is the pixel spatial location, and (t) is the temporal location of that pixel, or the frame number it is at. Similar to image regression task, we formulate this task as:

$$\Phi : \mathbb{R}^3 \mapsto \mathbb{R}^O \tag{10}$$

Where O is the dimension of the pixel color value of the video at the given pixel location at the given frame. We also supervise the model using MSE loss between the predicted color and ground truth color. There are two splitting strategies. In the first strategy we split all three dimensions of the input coordinates, for a set of coordinates in the format (x, y, t), we split it into (x), (y) and (t) and sample values in each separated channel. We denote this strategy as X+Y+T. In the second strategy, we only separate the pixel/spatial dimension with the frame/temporal dimension, for a set of coordinates in the format (x, y, t), we split it into (x, y) and (t) and sample values in each separated channel. We denote this strategy as XY+T.

In this experiment, we use 5-layer coordMLPs with 1024 hidden units to fit 2 10-second video clips[3], and we train for 100,000 epochs.

While performing our sampling strategy for CoordX with XY+T splitting mentioned in Sec. 4.1, for each training batch, we first randomly permute frame values and choosing the first t values to be the frames to sample. We sample 3.8% of the total points each batch, therefore for each frame we sample $y = 0.038N/t$ points (the number is rounded to the nearest integer), where N denotes the total number of points in the 3D space for the video. The coordinate values along the spatial (XY) dimension and the chosen frame values along the temporal (T) dimension for each sampled point are

[3]A bike video from http://www.scikit-video.org/stable/datasets.html, and a cat video from https://www.pexels.com

(a) X+Y, SIREN (b) SIREN (c) X+Y, PE (d) PE (e) Ground Truth

Figure 5: Qualitative results for the image fitting task. The 4 images shown are from the DIV2K dataset, center-cropped and down-sampled to a 512x512 resolution.

fed to CoordX. The sampling method for X+Y+T strategy is very much similar, except each chosen point is further split along the XY dimension. Like image fitting task, the model is supervised using a MSE loss of predicted color and ground truth color for each pixel.

We provide the qualitative results for the video fitting task in Fig 6 and 7, where we capture and show several frames of the two videos for comparison.

B.3 3D MODEL FITTING

We represent 3D shapes using an 1D occupancy grid (Mescheder et al., 2019), inspired by similar works in (Tancik et al., 2020). An occupancy grid represents the shape as a 1D occupancy probablity for a given 3D coordinate, and indicate whether the query points are inside or outside the 3D shape:

$$\Phi : \mathbb{R}^3 \mapsto \mathbb{R}^1 \tag{11}$$

For this task, we split the input coordinates along all three dimensions. We sample values along each of the three coordinate channels of the input 3D coordinates. We use 5-layer coordMLPs with 256 hidden units to fit 4 3D objects (Bunny, Armadillo, Dragon and Buddha) from The Stanford 3D Scanning Repository[4], and train each for 10,000 epochs. We follow the settings in Tancik et al. (2020), and use cross-entropy loss for the model to learn the classification of occupancy labels.

We first recenter points loaded from mesh points to $[-1, 1]$ for SIREN test. For each batch, we randomly choose a number of points to sample per axis. We store those sampled points and their

[4] http://graphics.stanford.edu/data/3Dscanrep/

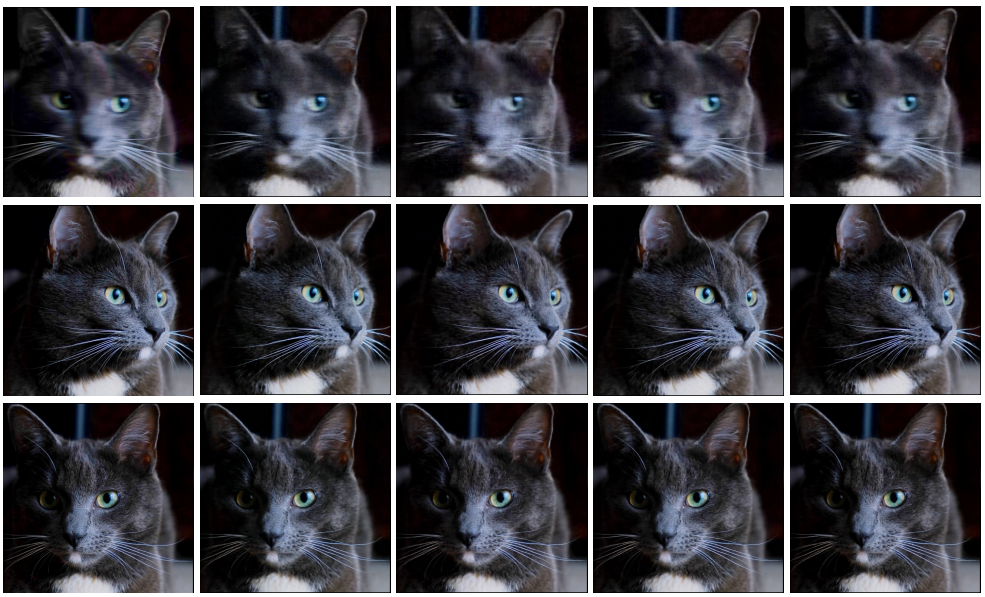

(a) Ground Truth (b) PE MLP (c) X+Y+T (d) XY+T (e) XY+T with split acceleration

Figure 6: Qualitative results for the video fitting task (the cat video).

(a) PE MLP

(b) X+Y+T

(c) XY+T

(d) XY+T with split acceleration

(e) Ground Truth

Figure 7: Qualitative results for the video fitting task (the bike video).

corresponding ground truth occupancy value to a file, to skip the time-consuming data sampling step, which acts as a major performance bottleneck in the training process, in order to present a more accurate results of our split acceleration.

C VOLUMETRIC RENDERING WITH COORDX

Volumetric rendering is another important application of coordinate-based MLPs in 3D graphics visualization. Unlike the previously discussed tasks which show good input data alignment (i.e., the input coordinates can be easily decomposed along each dimension), volumetric rendering application does not have this property in its sampled coordinates, e.g., Fig. 8. To enable CoordX's use in volumetric rendering tasks, we use an interpolation method that transforms the point sampling space into axis-aligned grids. The details of our solution will be discussed in the following sections.

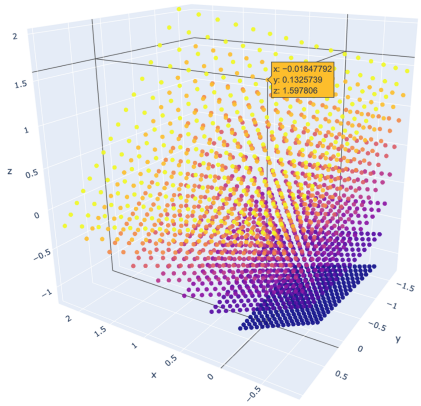

Figure 8: Illustration of sampled coordinate points for volumetric rendering.

C.1 VOLUMETRIC RENDERING

NeRF (Mildenhall et al., 2020) performs ray rendering during training and inference. It essentially renders a 2D image based on the camera ray from a given camera location. This method is derived from the classic volume rendering technique (Kajiya & Von Herzen, 1984) to render a 2D image given the camera location. The expected color $C(r)$ where $r(t) = o + td$ is the function representing ray from camera, with near and far bound t_n, t_f can be described as:

$$C(r) = \int_{t_n}^{t_f} T(t)\sigma(r(t)))c(r(t), d)dt \quad \text{where} \quad T(t) = \exp(-\int_{t_n}^{t} \sigma(r(s))ds) \tag{12}$$

To estimate this continuous integral shown in the Eqn. 12, NeRF uses a volume sampling technique, where 3D points are densely sampled along each camera ray, the color and volume density at each point are accumulated and used to predict the final color of the camera ray, in order to render the final image:

$$C(r) \approx \sum_{i=1}^{n} T(i)(1 - \exp(-\sigma_i \delta_i))c_i \quad \text{where} \quad T(i) = \exp(-\sum_{j=1}^{i-1} \sigma_j \delta_j) \tag{13}$$

Here δ_i is the distance between adjacent point samples t_i, t_{i-1}, c_i and σ_i is the color and volume density of the sampled point.

In real applications, hierarchical sampling is used for higher quality rendering. A coarse sampling is first performed so the rough depth information of the object can be obtained. Next, we do fine-grained sampling around the object surface based on estimated depth information.

C.2 RAY SAMPLING WITH A SPLIT MLP ARCHITECTURE

As explained in C.1, volume rendering includes casting a ray from the camera to each pixel of the rendered image, and sampled points along that ray. After that, each sampled coordinate point

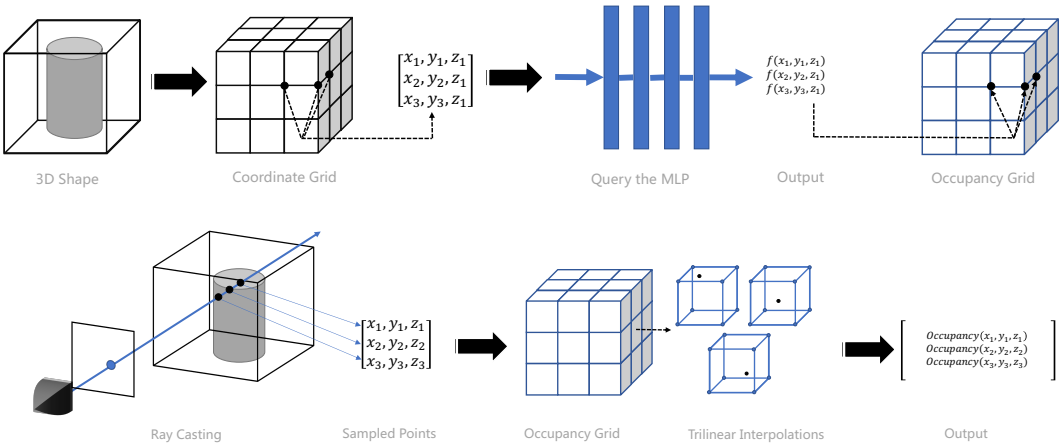

Figure 9: Illustration of our modified volumetric rendering.

is used as the input to the coordMLP, and it predicts a signal for each point. These predictions are then accumulated with other points on the same ray using rendering functions to generate the final color of the ray at that pixel. The difficulty of incorporating our coordX model with volume rendering is that the sampled points are not axis-aligned and cannot be decomposed along coordinate dimensions. Since the camera ray is usually not aligned with any of the x, y, z axis in 3D space, sampled points along the ray do not share coordinate values (Fig. 8). To address this problem, we use an interpolation-based rendering method which outputs predicted signal values of queried points by interpolating on a pre-computed grid. The interpolation based acceleration can also be seen in other relevant work such as FastNeRF (Garbin et al., 2021) and PlenOctrees (Yu et al., 2021).

As illustrated in Fig. 9, we first pre-compute a 3D occupancy grid for the 3D object with pre-defined resolution (e.g., 256). Each voxel inside the grid occupies a small cubic space. After pre-computation, if we are to render an image from an arbitrary camera angle, we can perform interpolation-based volumetric rendering, where the occupancy of the points we sampled along each ray is trilinearly interpolated from the 8 endpoints of the voxel cube which this point is in. We then get accumulated color/depth for each ray using the original volumetric rendering methodology.

Based on this interpolation raycasting method, we can replace the baseline CoordMLP with our CoordX model to accelerate the grid pre-computation step (the most time-consuming step in the whole processing pipeline). The points in the pre-computed 3D coordinate grid can be decomposed into 3 vectors which are used to query CoordX. We demonstrate a 2.8x speedup with CoordX in Fig. 3(c).

A similar approach can be used to accelerate training for NeRF models. However, using grid interpolation for training requires training with all the points in the grid, which can be much larger than the number of points required to train the baseline model. Thus our grid interpolation-based training may consume more memory and take longer training times. To address this problem, we decide to first compute the split features just before fusion for the corresponding grid. For each query point, bilinear interpolation is performed directly on these split features, the interpolated features will then be fed into the second part of our splitting model to predict final signal values. In this way, we strike a balance between grid reuse and computation efficiency.

C.3 Experimental Evaluation

Visualization of learned 3D occupancy. We apply our proposed rendering method to MLP models for 3D occupancy representations trained in 4.1. We choose the original volumetric rendering method as the baseline rendering method. We choose 512×512 as the target resolution of the rendered images. We uniformly sample 256 points along the ray for each level of two granularity levels in hierarchical rendering. The coordinate grid used in our grid interpolation rendering method has the resolution of 384 for the longest length of the object's 3D bounding box. Fig. 9 shows the qualitative comparison of the rendered images. Our grid interpolation based rendering is referred to

as grid in the figure. The Table 6 shows the speed comparison of different rendering method. We test the time required to render one image (including the time to pre-compute the grid for our method).

We make the following observations. First, grid interpolation rendering can achieve significant speedups compared to baseline volumetric rendering (2.70x and 14.83x for baseline and CoordX respectively). Second, with our grid inperpolation rendering, CoordX achieves a 2.15x speedup over the baseline MLP. Third, the rendered images in Fig. 9 show our rendering method is able to render high quality images for different MLP models.

Model	baseline MLP		CoordX	
Rendering Method	baseline	grid	baseline	grid
$T_{\text{rendering}}$ (sec)	6.61	2.45	16.91	1.14

Table 6: Rendering time comparison for different volumetric rendering method.

Novel View Synthesis We train a simplified 8-layer NeRF model for the Lego bulldozer scene. We use the spherical harmonics (SH) function proposed in Yu et al. (2021) to decompose the point position and view direction so that the input to the NeRF MLP is just the positional coordinates (x, y, z). We refer to this model as our baseline NeRF model. Our CoordX NeRF model is based on this baseline model. We split the positional coordinates (x, y, z) in 3 branches and 2 FC layers are kept after the fusion operation ($D_s = 6, D_f = 2$). The resolution of the feature grid used for bilinear interpolation is set to 384.

To train these NeRF models, we use downsampled ground truth images (400×400) for supervised learning. 128 points are sampled along randomly selected rays. For simplicity, we do not use hierarchical sampling for NeRF models. The models are trained for 200,000 epochs. To visualize the scene learned by NeRF models, we evaluated both baseline volumetric rendering and grid interpolation rendering (similar to 3D shape rendering). The target resolution of the rendered images is 400×400. The coordinate grid used has a resolution of 384 for the longest length of the object's 3D bounding box. We sample 256 points along the ray (without hierarchical sampling). The PSNR is evaluated based on these rendered images. Table 7 compares the baseline NeRF and CoordX NeRF from different aspects, and Fig. 11 shows the rendered images for qualitative comparison.

Metrics	PSNR		$T_{\text{rendering}}$ (sec)		T_{training} (hr)
	baseline	grid	baseline	grid	
baseline-NeRF	29.65	29.23	3.09	1.97	4.73
CoordX-NeRF	29.29	28.98	7.82	0.70	2.61

Table 7: Quantitative comparison between baseline NeRF and our CoordX NeRF.

We make the following observations. First, our proposed interpolation-based training can help CoordX achieve a 1.81x training speedup over baseline NeRF. Second, our CoordX NeRF model achieve similar PSRN scores (less than 0.5 PSNR drop) compared to the baseline NeRF. Third, our grid interpolation rendering method can achieve the same level of rendering accuracy (less than 0.5 PSNR drop) compared to the original rendering method for both baseline and CoordX models.

In summary, we demonstrate that our proposed grid interpolation method is able to render images with comparable quality with significant rendering speedups. This method also enables our CoordX model to achieve training and inference acceleration over the baseline model.

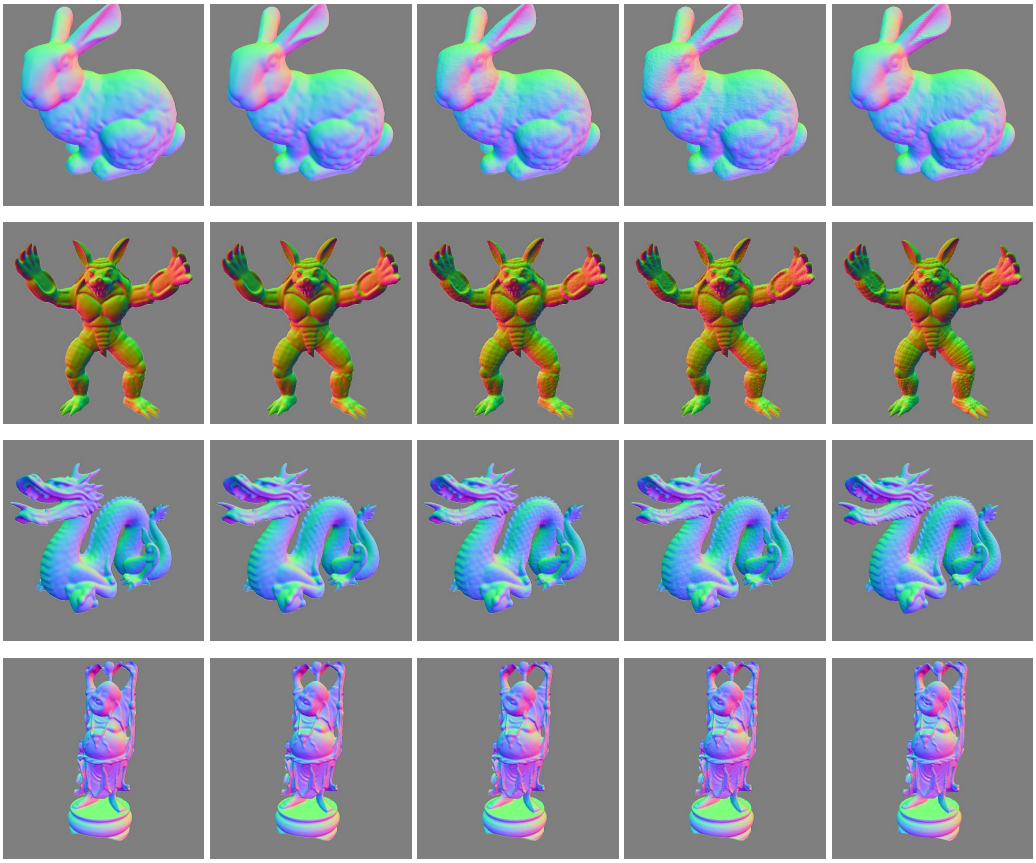

(a) MLP baseline (b) MLP grid (c) CoordX grid (d) CoordX-A grid (e) Ground Truth

Figure 10: Images result rendered using different ray rendering methods.

(a) NeRF baseline (b) NeRF grid (c) CoordX baseline (d) CoordX grid (e) Ground Truth

Figure 11: Images rendered using NeRF.